Nonperturbative calculation of charge-changing processes in C^{4+} scattering from neon atoms

T. Kirchner,[1] M. Horbatsch,[1] and H. J. Lüdde[2]
[1]*Department of Physics and Astronomy, York University, Toronto, Ontario, Canada M3J 1P3*
[2]*Institut für Theoretische Physik, Universität Frankfurt, Robert-Mayer-Straße 8, D-60054 Frankfurt/Main, Germany*
(Received 5 February 2001; published 7 June 2001)

Total cross sections for single- and multiple-electron capture and ionization events in $C^{4+}+Ne$ collisions are calculated in the independent particle model using the nonperturbative basis generator method. Dynamical screening effects due to the removal of electrons from the target atom and due to the capture of electrons to the projectile ion are taken into account in a global fashion. Our data for impact energies from 20 to 2000 keV/amu follow the trends of previous calculations for proton and He^{2+} impact, in particular with respect to the energy dependence of the net electron loss from the target. When comparing our results to available experimental total cross sections for C^{4+} and F^{4+} impact, we find that (1) relative populations of recoil ion charge states are generally well reproduced; (2) the absolute normalizations of experimental data appear to be problematic; and (3) charge-state correlated cross sections are in agreement for processes including up to two electrons, but discrepancies persist for higher electron multiplicities. It is argued that new experimental investigations of global and charge-state correlated cross sections would be helpful to further the understanding of ion-atom collision systems with many active electrons in the regime of medium impact energies.

DOI: 10.1103/PhysRevA.64.012711 PACS number(s): 34.50.Fa, 34.10.+x, 34.70.+e

I. INTRODUCTION

Numerous experimental results for the production of recoil ions in collisions between multiple charged ions and noble gas atoms have been reported in the literature since the first measurements more than 20 years ago [1]. The body of data includes net electron loss cross sections, cross sections for the production of recoil ions in specific charge states, and cross sections for simultaneous capture and ionization events, which are obtained from measuring the final charge states of the recoil and the projectile ions in coincidence.

Most of the data were collected in the 1980's and are reviewed in Ref. [2]. With the advent of recoil ion momentum spectroscopy [3], the main course of research in the field has shifted to more differential studies in recent years, leaving some issues in the investigation of total cross sections unresolved. In particular, the experimental data for target atoms heavier than helium are mainly restricted to collisions of multiple charged projectiles at impact energies around 1 MeV/amu or higher. Measurements at intermediate energies, where the projectile velocity is comparable to the mean velocity of the outermost bound target electrons are rare, and systematic studies of the energy dependence of global and charge-state correlated cross sections were only reported for proton [4] and helium-ion [5] impact. Scaling laws have been frequently applied to extrapolate measured data to this region (see, e.g., Ref. [6]) but it is difficult to assess the accuracy of the cross sections obtained in this way.

On the theoretical side, early attempts to explain the experimental results in the nonperturbative realm were based on classical [7] and statistical [1] models. Refined versions of the early models were successful in describing various gross features of the measured cross-section data [2,8,9] and in guiding the general understanding of the collision processes. However, they suffer from some inherent limitations, such as the wrong energy dependence of the total ionization cross section at high energies and the inability to account for resonant charge transfer in the classical trajectory Monte Carlo (CTMC) method [10].

Quantum-mechanical calculations for the description of the experimental data on a more quantitative level have been reported only relatively recently. As the explicit solution of the many-electron time-dependent Schrödinger (or Dirac) equation that governs the collision dynamics is prohibitive for most situations of interest, the quantal descriptions usually start from an effective single-particle picture, in which the electron-electron interaction is described by a (generally) time-dependent, mean-field potential. Such independent-particle-model (IPM) calculations are computationally expensive when the mean-field potential is chosen to account for dynamical screening and exchange effects on a microscopic level, such as in the time-dependent Hartree Fock (TDHF) theory [11] or in approximate schemes of time-dependent density-functional theory (TDDFT) [12]. Furthermore, the nonlinearity of the TDHF or TDDFT Hamiltonian causes fundamental theoretical problems, which usually manifest themselves in fluctuating transition probabilities at asymptotic times after the collision [13]. As a consequence, only a few calculations for ion-atom collisions with more than two active electrons have been performed on this level [14].

In recent work, we have approached the problem at hand in the IPM with a single-particle potential that accounts for electronic screening and exchange effects in the ground state of the target atom, but neglects the response of the electronic density in the presence of the projectile [15]. A large number of one- and two-electron processes in collisions of singly and doubly charged ions with atoms can be calculated successfully in this *no-response* approximation over a broad range of impact energies, provided that the time-dependent, single-particle equations are solved accurately, and the resulting single-particle probabilities for the various processes are combined appropriately to evaluate cross sections for multiple-electron transitions [16,17]. Moreover, we have de-

veloped a model to include dynamical screening effects due to the removal of electrons from the target atom in a global fashion [18]. This *target-response* model proved capable of improving the results for multiple-electron processes and furthermore allowed an analysis and solution of the TDHF (or TDDFT) projection problem mentioned above. The model does not increase the computational cost significantly, compared to a calculation in the *no-response* approximation.

In the present paper we extend our investigations to the $C^{4+}+Ne$ collision system with the aim to assess the validity of the IPM description and the importance of response effects for a more highly charged projectile ion. Multiple capture is likely to be important at low to intermediate impact energies due to the relatively high projectile charge. Thus, we extend the global model for response effects to account for the screening of the projectile ion during the collision, while electron density is transferred from the target. As in our previous work, the single-particle equations are propagated with the basis generator method (BGM) [19]. The evaluation of probabilities for charge-changing processes is based on the analysis in terms of products of binomials [17], which was introduced as an alternative to standard trinomial statistics to overcome the problem of unphysical higher-order capture events. The results are compared with the limited experimental data for $C^{4+}+Ne$ collisions [20] and with measurements for F^{4+} impact [21,22]. The latter system should have comparable global cross sections, but, as will be discussed below, may differ from the C^{4+} projectile case for charge-state correlated events.

II. THEORY

A. Time-dependent screening models

For the $C^{4+}+Ne$ collision system, we assume that the electrons at the projectile center are passive and occupy the tightly bound $1s^2$ state throughout the collision. They enter the description only by providing a frozen screening potential to be added to the Coulomb potential of the projectile nucleus. In the IPM, the (nonrelativistic) scattering system is then represented by a set of time-dependent single-particle equations for the initially occupied target orbitals (we use atomic units, i.e., $\hbar=m_e=e=1$)

$$i\partial_t\psi_i(\mathbf{r},t)=\hat{h}(t)\psi_i(\mathbf{r},t),\quad i=1,\ldots,N, \tag{1}$$

with the Hamiltonian

$$\hat{h}(t)=-\frac{1}{2}\Delta+v^T_{\rm eff}(\mathbf{r},t)+v^P_{\rm eff}(\mathbf{r},t). \tag{2}$$

The effective potentials at the target and projectile centers $v^T_{\rm eff}$ and $v^P_{\rm eff}$ can be decomposed into nuclear parts and contributions due to the electron-electron interaction in the undisturbed ground-state orbitals before the collision and due to the time-dependent variation of the electronic system during the collision

$$v^T_{\rm eff}(\mathbf{r},t)=-\frac{Z_T}{r}+v^T_{ee}(r)+\delta v^T_{ee}(\mathbf{r},t)=v^T_0(r)+\delta v^T_{ee}(\mathbf{r},t), \tag{3}$$

$$v^P_{\rm eff}(\mathbf{r},t)=-\frac{Z_P}{r_P}+v^P_{ee}(r_P)+\delta v^P_{ee}(\mathbf{r},t)=v^P_0(r_P)+\delta v^P_{ee}(\mathbf{r},t). \tag{4}$$

Here, Z_T and Z_P denote the charges of the target and projectile nuclei, respectively. We assume that the projectile ion moves along the classical straight line trajectory $\mathbf{R}(t)=(b,0,v_Pt)$ with impact parameter b and constant velocity v_P, and choose the target center as the origin of the reference frame. The coordinate of the electron with respect to the target center is denoted by $\mathbf{r}$, while the distance between the electron and the projectile center is $r_P=|\mathbf{r}-\mathbf{R}(t)|$.

As in our previous work, we use the *exchange-only* version of the optimized potential method (OPM) [23] to represent the undisturbed atomic target potential $v^T_0(r)$. In the OPM, self-interaction contributions contained in the Hartree energy are canceled exactly, and the correct asymptotic behavior $v^T_0(r)\to-1/r$ is ensured.

To represent the screening of the nucleus in the $C^{4+}(1s^2)$ projectile, we use the model potential

$$v^P_{ee}(r_P)=\frac{N_P}{r_P}[1-(1+\alpha r_P)\exp(-2\alpha r_P)], \tag{5}$$

where N_P is the number of core electrons ($N_P=2$ in our case) and α is an adjustable parameter. This potential behaves as N_P/r_P asymptotically such that the total projectile potential v^P_0 has a $-Q_P/r_P$ tail with the asymptotic charge $Q_P=Z_P-N_P$. Following other studies involving screened projectiles [24], we choose α such that the orbital binding energy of an additional electron in the $2s$ state is adjusted to the ionization potential (IP) of $C^{3+}(1s^22s)$. Using the value of IP$=2.370$ a.u. [25] we find $\alpha=3.7276$.

We define the *no-response* approximation, in which dynamical screening and exchange effects are completely neglected by

$$\delta v^T_{ee}(\mathbf{r},t)=\delta v^P_{ee}(\mathbf{r},t)=0. \tag{6}$$

This approximation is justified at high-impact energies, and was used in previous studies for singly and doubly charged projectiles. It was shown to be valid for single-electron transitions, such as single capture and single ionization down into the tens of keV/amu range [16,17]. We found that dynamical screening effects become important for multiple-electron transitions at impact energies below 500 keV/amu, and thus, they also influence the global net electron capture and ionization cross sections, in which the individual cross sections for q-fold ionization and capture are added according to their multiplicities q [18].

In order to include time-dependent screening in the calculation without increasing the computational cost compared to the *no-response* approximation we devised a relatively simple model, in Ref. [18]. In this model, the total effective target potential is approximated by a linear combination of

ionic ground-state potentials v_q^T. These are weighted with the time-dependent probabilities $P_q^{\rm loss}(t)$ to create the corresponding charge state in the collision, i.e.,

$$v_{\rm eff}^T(\mathbf{r},t)\approx\sum_{q=0}^{N} P_q^{\rm loss}(t)v_q^T(r). \tag{7}$$

The ionic potentials are expressed by the potential of the undisturbed target atom scaled to yield the asymptotic behavior of the desired charge states

$$v_q^T(r)=\begin{cases} v_0^T(r) & \text{for} \quad q=0 \\ v_0^T(r)-\dfrac{q-1}{N-1}v_{ee}^T(r) & \text{for} \quad q\geqslant 1. \end{cases} \tag{8}$$

This ansatz yields the same potentials for $q=0$ and $q=1$, and was guided by the idea to account for dynamical screening in the case of multiple-electron processes, but to suppress it in the kinematical range where zerofold to onefold electron removal dominates. We note, however, that this can only be achieved approximately due to the statistical nature of the description, in which all channels are described by a single mean-field potential.

With the relation

$$P_0^{\rm loss}(t)=1-\sum_{q=1}^{N} P_q^{\rm loss}(t), \tag{9}$$

and the definition of the net electron loss

$$P_{\rm net}^{\rm loss}(t)=\sum_{q=1}^{N} qP_q^{\rm loss}(t), \tag{10}$$

the response potential $\delta v_{ee}^T(t)$ in Eq. (3) can be written as

$$\delta v_{ee}^T(\mathbf{r},t)\approx-\frac{P_{\rm net}^{\rm loss}(t)+P_0^{\rm loss}(t)-1}{N-1}v_{ee}^T(r). \tag{11}$$

This model accounts for the increasing attraction of the effective potential $v_{\rm eff}^T$ as electrons are removed from the target during the collision. To incorporate the time-dependent screening of the projectile ion due to capture processes, we now construct a response potential $\delta v_{ee}^P(t)$ in a similar fashion. The total effective projectile potential $v_{\rm eff}^P$ [Eq. (4)] is written as the linear combination

$$v_{\rm eff}^P(\mathbf{r},t)\approx\sum_{k=0}^{M_P} P_k^{\rm cap}(t)v_k^P(r_P), \tag{12}$$

where $P_k^{\rm cap}(t)$ is the time-dependent probability for k-fold capture, and v_k^P is the ionic ground-state potential that is experienced by the kth electron to be captured. M_P denotes the number of electrons that can be captured by the projectile ($M_P=4$), which is less than the number N of electrons available at the target in our case. Here, we have followed the idea of the analysis of multiple capture and ionization events in terms of products of binomials [17]. In this model, capture of higher multiplicities than M_P is prohibited by distributing the net-electron capture probability $P_{\rm net}^{\rm cap}(t)$ over the physically allowed channels according to

$$P_k^{\rm cap}(t)=\frac{M_P!}{k!(M_P-k)!}\left(\frac{P_{\rm net}^{\rm cap}(t)}{M_P}\right)^k\left(1-\frac{P_{\rm net}^{\rm cap}(t)}{M_P}\right)^{M_P-k}. \tag{13}$$

The ionic potentials v_k^P in Eq. (12) are modeled in analogy to Eq. (8) as

$$v_k^P(r_P)=\begin{cases} v_0^P(r_P) & \text{for} \quad k=0 \\ v_0^P(r_P)+\dfrac{k-1}{2}v_{ee}^P(r_P) & \text{for} \quad k\geqslant 1. \end{cases} \tag{14}$$

Again, this choice aims at a suppression of dynamical screening effects in the case of zerofold and onefold capture. For increasing k, the asymptotic charge of the ionic potential is reduced by one unit such that a singly charged potential is obtained for $k=M_P=4$ (with the charge balance $Q_P=M_P$).

Inserting Eq. (14) into Eq. (12) and noting

$$P_0^{\rm cap}(t)=1-\sum_{k=1}^{M_P} P_k^{\rm cap}(t) \tag{15}$$

$$P_{\rm net}^{\rm cap}(t)=\sum_{k=1}^{M_P} kP_k^{\rm cap}(t), \tag{16}$$

we find for the response potential $\delta v_{ee}^P(t)$ in Eq. (4)

$$\delta v_{ee}^P(\mathbf{r},t)\approx\frac{P_{\rm net}^{\rm cap}(t)+P_0^{\rm cap}(t)-1}{2}v_{ee}^P(r_P). \tag{17}$$

The parameter α in the effective potential v_{ee}^P [Eq. (5)] was adjusted to fit the ionization potential of the C^{3+} ion in order to provide a reasonable screening potential for the first electron to be captured. In the case of multiple capture, for which the response potential (17) is turned on, this choice is questionable as the additional electrons are captured into more weakly bound states. To account for this change in the effective potential we use a different parameter $\tilde{\alpha}$ for v_{ee}^P in Eq. (17). We choose $\tilde{\alpha}=1.8523$ to obtain $\varepsilon_{2s}=-1.760$ a.u. which fits the ionization potential of C^{2+} [25] and adjusts the response potential to the most likely multiple-capture channel, i.e., twofold capture. Of course, this choice can also be criticized, since we always find a mixture of all allowed k-fold capture channels in a mean-field description. In practice, this ambiguity proved to be unimportant as calculations with either $\tilde{\alpha}=3.7276$ or $\tilde{\alpha}=1.8523$ in v_{ee}^P in Eq. (17) yielded very similar results.

B. Calculational details

To solve the single-particle equations (1) in the *no-response* approximation [Eq. (6)] and with inclusion of target- and projectile-response effects [Eqs. (11) and (17), respectively] we use the same BGM expansion as in our previous works [18,26]

$$|\psi_i(t)\rangle = \sum_{\mu=0}^{M} \sum_{v=1}^{V} c^i_{\mu v}(t) |\chi^\mu_v(t)\rangle, \tag{18}$$

$$|\chi^\mu_v(t)\rangle = [W_P(t)]^\mu |\varphi^T_v\rangle \quad \mu = 0, \ldots, M, \tag{19}$$

$$W_P(t) = \frac{1}{r_P}[1 - \exp(-r_P)]. \tag{20}$$

The basis includes all undisturbed target eigenstates $|\varphi^T_v\rangle$ of the $KLMN$ shells [i.e., $v=1,\ldots,V$ in Eq. (18) corresponds to $v=1s,\ldots,4f$), and also 100 functions from the set $\{|\chi^\mu_v(t)\rangle, \mu \geqslant 1\}$ up to order $\mu = M = 8$.

The inclusion of the response potentials (11) and (17) requires knowledge of the net electron loss $P^{\rm loss}_{\rm net}$ and the net electron capture $P^{\rm cap}_{\rm net}$ in each time step of the propagation. Both quantities can be defined by sums over occupied channel functions for attachment to the target and projectile centers. It has been observed in several TDHF calculations that the use of undisturbed eigenstates of the projectile and target systems as channel functions may lead to transition probabilities that fluctuate for all times [13]. This projection problem is associated with the nonlinearity of the TDHF Hamiltonian. As a solution, we proposed a different analysis in Ref. [18], in which the propagated orbitals are projected onto the eigenfunctions of the Hamiltonian, which includes dynamical screening effects. We tested this idea for the target-response potential (11) and obtained stable transition probabilities, and, in particular, a stable net electron loss when projecting the solutions of Eq. (1) onto the eigenstates $|\varphi^T_v(t)\rangle$ which satisfy

$$\left(-\frac{1}{2}\Delta - \frac{Z_T}{r} + v^T_{ee}(r) + \delta v^T_{ee}(r,t)\right)|\varphi^T_v(t)\rangle = \varepsilon_v(t)|\varphi^T_v(t)\rangle. \tag{21}$$

The states $|\varphi^T_v(t)\rangle$ are consistent with the time-dependent, mean-field description, as they correspond to the average fractional charge state of the target atom after the collision. We diagonalize the Hamiltonian of Eq. (21) in the BGM basis to represent the states $|\varphi^T_v(t)\rangle$ and calculate the net electron loss according to

$$P^{\rm loss}_{\rm net}(t) = N - \sum_{i=1}^{N} \sum_{v=1}^{V} |\langle \varphi^T_v(t)|\psi_i(t)\rangle|^2. \tag{22}$$

It proved sufficient to sum over the population of the first 20 states $|\varphi^T_v(t)\rangle$ in Eq. (22) [18].

In principle, the inclusion of the projectile-response potential (17) requires an analogous procedure to calculate the net electron capture. However, this cannot be handled straightforwardly in the present implementation of the BGM, in which no projectile states are included in the basis explicitly. Capture probabilities are calculated after the time-propagation is completed by projecting the stored time-dependent orbitals $|\psi_i(t)\rangle$ onto moving eigenstates of the projectile ion. This projection can be done for each desired internuclear separation, and hence, the net electron capture defined with respect to the traveling projectile states $|\varphi^P_k(t)\rangle$

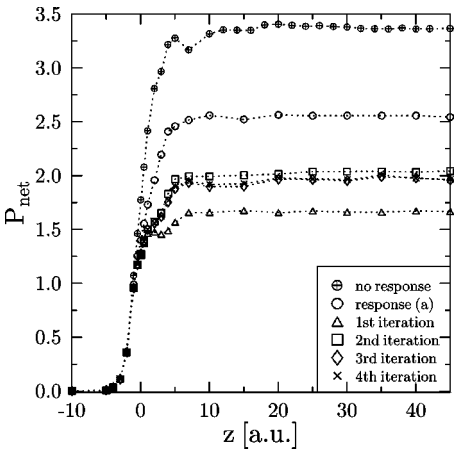

FIG. 1. Net electron capture probability $P^{\rm cap}_{\rm net}$ (23) as a function of the scaled time $z = v_P t$ at $E_P = 20$ keV/amu and $b = 1.75$ a.u. in $C^{4+} + Ne$ collisions. The calculations are explained in the text.

$$P^{\rm cap}_{\rm net}(t) = \sum_{i=1}^{N} \sum_{k=1}^{K} |\langle \varphi^P_k(t)|\psi_i(t)\rangle|^2, \tag{23}$$

can be calculated as a function of time. However, this $P^{\rm cap}_{\rm net}(t)$ is not available simultaneously with the propagated orbitals $|\psi_i(t)\rangle$ in the present computer code and cannot be used directly for the construction of the projectile-response potential (17).

To solve this technical problem, we have devised an iterative procedure for the inclusion of projectile-response effects. In the first step, we solve the time-dependent, single-particle equations (1) with the target-response potential (11) only. The propagated orbitals $|\psi_i(t)\rangle$ are stored at many discrete time steps during the collision to calculate the net electron capture according to Eq. (23) as a function of time. We note that we have subtracted the bound target part of the orbitals $|\psi_i(t)\rangle$ before the projection is carried out in order to avoid the problem of overlapping projectile and target states around the closest approach. In the second step (the first iteration) we repeat the time-propagation with inclusion of the target- and the projectile-response potentials, where the latter is calculated with the time-dependent net electron capture function of the first step as input. From the second propagation we obtain a new net electron capture, which is used as input for a third step (second iteration), etc. The steps are repeated until the net electron capture function $P^{\rm cap}_{\rm net}(t)$ converges.

Figure 1 illustrates this procedure for $C^{4+} + Ne$ collisions at the projectile energy $E_P = 20$ keV/amu and the impact parameter $b = 1.75$ a.u. $P^{\rm cap}_{\rm net}(t)$ is calculated at 36 internuclear separations by projection onto the undisturbed eigenfunctions of the LMN shells of the C^{4+} ion defined by the Coulomb potential of the nucleus and the effective potential (5) [i.e., $k=1,\ldots,K$ in Eq. (23) corresponds to $k=2s,\ldots,4f$]. Note that the occupied projectile K-shell states are not included in the projection. $P^{\rm cap}_{\rm net}(t)$ is interpolated to all time steps of the propagation when used as input for the projectile-response potential in the iteration. Figure 1 shows that $P^{\rm cap}_{\rm net}(t)$ obtained in the *no-response* approxima-

tion [Eq. (6)] is reduced by approximately 25% when the target-response potential is included [response(a)]. When this $P_{\rm net}^{\rm cap}(t)$ is used to calculate the projectile-response potential in the first iteration, the projectile is screened considerably during the time propagation and, as a consequence, a smaller amount of density is transferred from the target. The new $P_{\rm net}^{\rm cap}(t)$ implies a degraded dynamical screening of the projectile in the next step and leads to a somewhat larger $P_{\rm net}^{\rm cap}(t)$ after the second iteration. Convergence at the 1% level is achieved after the third to fourth iteration. In total, the inclusion of the projectile-response potential reduces the net electron capture by an additional 17% of the *no-response* result for the example shown in Fig. 1.

The dynamical projectile screening also affects the net ionization defined as the difference of net electron loss (22) and capture (23). For the particular situation depicted in Fig. 1, the ionization of the *no-response* calculation is reduced due to target response by about one half, but is increased again, when the projectile-response potential is included, such that after the fourth iteration, 75% of the *no-response* result is obtained. This demonstrates that a part of the electron density, which is captured into bound states when the projectile potential is frozen, is transferred to the continuum when dynamical screening on the projectile center is included.

Finally, we note that $P_{\rm net}^{\rm cap}(t)$ does not fluctuate significantly as a function of time, although we have projected onto the undisturbed eigenfunctions of the C^{4+} ion in each step of the iteration. By contrast, we find an oscillating net electron loss, when the bound target part is analyzed with respect to the undisturbed eigenstates of the neon atom [18]. This different behavior at both centers might be related to the fact that the BGM is built upon a target-centered basis only. There is no *a priori* reason why the projection problem should be of minor importance for dynamical screening effects on the projectile center, as the theoretical analysis presented in Ref. [18] applies to this case as well.

III. RESULTS AND DISCUSSION

In this section, we discuss our results for charge-changing processes in $C^{4+}+Ne$ collisions in comparison with experimental data. The total cross section for net electron loss from the target σ_+ is shown in Fig. 2. While the inclusion of the target-response potential reduces the *no-response* cross section at low to intermediate impact energies significantly, the additional dynamical screening of the projectile changes the target-response results at most at the 10% level at the lowest energy $E_P=20$ keV/amu. The effect of the projectile response is pronounced at intermediate impact parameters [cf. Fig. 1], but it is small at larger impact parameters, which contribute considerably to the net electron loss cross section. We have also included theoretical results obtained in the *no-response* and *target-response* models for $Be^{4+}+Ne$ collisions to assess the role of the passive electrons in the C^{4+} projectile. These cross sections are slightly smaller than the results for C^{4+} impact, due to the fact that in the case of C^{4+} impact, a larger effective projectile charge is experienced by the target electrons at small internuclear separations. The small difference justifies a comparison of our results with experimental data obtained for C^{4+} [20,27,28] and F^{4+} [21,22] projectiles. In the case of F^{4+} impact, only cross sections for charge-state correlated processes were reported in Refs. [21,22]. We added these cross sections according to their multiplicities to obtain σ_+. Our results are in good agreement with the experimental data of Refs. [22,27,28] around the impact energy $E_P=1000$ keV/amu, but the measurements at lower-impact energies do not follow the monotonic rise of the calculated cross section curve. Instead, they hint at a structured energy dependence with a minimum around $E_P=250$ keV/amu.

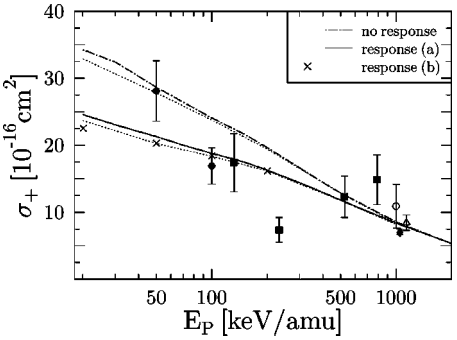

FIG. 2. Total cross section for net electron loss as a function of impact energy. Theory: present calculations for $C^{4+}+Ne$ collisions in the *no-response* approximation [Eq. (6)], with inclusion of the target-response potential (11) [response(a)] only, and with the additional projectile-response potential (17) [response(b)]. The dotted curves correspond to calculations for $Be^{4+}+Ne$ collisions in the no-response and response (a) models. Experiment: C^{4+} projectiles; (●) [20], closed diamond [28], (△) [27]; F^{4+} projectiles; closed squares [21], (○) [22].

In order to underpin the smooth impact-energy dependence of our results and to show that the behavior of the experimental data is likely to be flawed, we plot σ_+ divided by the projectile charge Q_P as a function of E_P/Q_P in Fig. 3. Measurements for other projectiles according to Table I and BGM calculations for proton [16] and He^{2+} [17] impact are

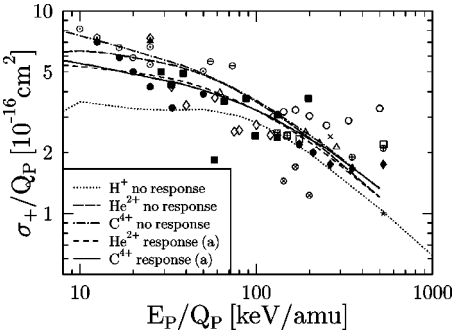

FIG. 3. Reduced plot of total cross sections σ_+ for the net recoil ion production divided by the projectile charge as a function of impact energy divided by projectile charge for Ne targets. Theory: present calculations for C^{4+} impact with and without inclusion of the target-response potential [response (a)] denoted by the full curve and chain curve, respectively; He^{2+} impact: [18]; H^+ impact: [16]. The symbols correspond to experimental data listed in Table I.

TABLE I. Sources of the experimental data used in Fig. 3.

Symbol	Projectile ion	Impact energy (kev/amu)	Reference
●	C^{2+}, C^{3+}, C^{4+}, C^{5+}	50, 100	[20]
⊙	Ne^{2+}, Ne^{3+}, Ne^{4+}, Ne^{5+}	50, 100	[20]
■	F^{4+}, F^{6+}, F^{8+}	130–790	[21]
○	F^{2+}, F^{3+}, F^{4+}, F^{5+}, F^{6+}, F^{7+}, F^{8+}	1000	[22]
△	C^{4+}, C^{5+}, C^{6+}	310, 1140	[27]
⋆	He^{2+}	1050	[28]
◆	C^{2+}, C^{3+}, C^{4+}, C^{5+}, C^{6+}	1050	[28]
⊕	O^{2+}, O^{3+}, O^{5+}, O^{6+}, O^{7+}, O^{8+}	1050	[28]
□	Ne^{2+}, Ne^{6+}, Ne^{7+}, Ne^{8+}	1050	[28]
×	Ar^{4+}, Ar^{6+}	1050	[28]
◇	Ne^{3+}	75–360	[29]
▲	N^{2+}	50	[33]
⊖	Cu^{6+}, Cu^{8+}	440	[33]
⊗	C^{5+}, C^{6+}, O^{7+}	1000	[34]

also included. Such a plot was first motivated by results of CTMC calculations, which reduce to a single curve for a given target atom in the scaled coordinates [27], and was subsequently used by experimentalists to compare their measurements [20,29,30]. We have not included the CTMC calculations of Ref. [27] in Fig. 3, since they were obtained in a different kinematical region with absolute impact energies ranging from 1 to 5 MeV/amu and projectile charges between $Q_P=5$ and $Q_P=80$. We note that the relevant curve in Fig. 7 of Ref. [27] shows a σ_+/Q_P of 1.2×10^{-15} cm^2 at $E_P/Q_P=10$ keV/amu, which lies about a factor of two above our result obtained with the target-response potential. At the highest reduced energies shown, the CTMC cross section lies slightly below our proton result, which in turn, is substantially below our data for $Q_P=2$ and $Q_P=4$. The experimental data included in Fig. 3 were selected from the literature with the constraints $E_P\lesssim1000$ keV/amu and $Q_P\leqslant8$.

The calculated cross sections for C^{4+} and He^{2+} impact are in close agreement in this reduced plot, in particular, when the target-response potential is included. We do not show results obtained with the inclusion of the projectile-response potential in Fig. 3, since they modify the target-response cross sections only slightly. We have checked at a few low and intermediate reduced impact energies that BGM calculations with target response for more highly charged ion impact (up to $Q_P=8$) deviate from the He^{2+} and C^{4+} data at most at the 10% level.

This close agreement, which implies an effective scaling of the net electron loss cross section is remarkable, as the capture and ionization contributions differ considerably for the various projectile charges and absolute energies in this kinematical range. For example, for a fixed reduced energy E_P/Q_P one observes that the capture contribution to the net electron loss decreases with increasing projectile charge Q_P, while the ionization contribution increases. Note that this is due to the increase in collision velocity v_P for fixed E_P/Q_P. Also, the impact parameter dependence of the net electron loss changes with Q_P, namely, the distribution flattens as larger b values contribute more for higher v_P.

At higher reduced impact energies, the He^{2+} and C^{4+} results diverge. This is due to the fact that the BGM calculations approach the limit of first-order perturbation theory, in which the energy dependence is given by $E_P^{-1}\ln E_P$ rather than by E_P^{-1}. In fact, our results for proton, He^{2+}, and C^{4+} projectiles merge when the reduced cross section σ_+/Q_P is plotted as a function of $E_P/(Q_P\ln E_P)$. We conclude that our present results for $C^{4+}+Ne$ collisions are consistent with our earlier data for proton and He^{2+} impact, which in turn, showed very good agreement with experimental data over a broad range of impact energies [16,18]. These measurements are not included in Fig. 3 for the sake of clarity.

The experimental data scatter considerably around the present theoretical results, but they do not indicate a structure in the cross section. Clearly, the data point of Ref. [21] for F^{4+} impact at $E_P/Q_P=57.5$ keV/amu (which is located at $E_P=230$ keV/amu in Fig. 2) is outside of a band suggested by the majority of the experimental data points. The rather inconclusive behavior of the experimental data included in Fig. 3 can be partly explained by the different screened projectile ions used in these measurements. In Ref. [28], it was argued that the cross sections for dressed projectiles should be scaled with respect to an effective charge $Q_{\rm eff}>Q_P$ to account for the higher charge of the projectile nuclei. For example, this procedure shifts the data points around 500 keV/(Q_P amu) to smaller reduced energies and smaller-reduced cross sections. However, it does not change the position of data points at low and intermediate reduced energies, considerably. New precise measurements for bare ion impact or for projectiles, for which the dressing effect is small (such as C^{4+}) are desirable to clarify the situation in this region and to assess the validity of our calculations on a quantitative level.

As mentioned above, the relative contributions of net electron capture $\sigma_{\rm cap}$ and net ionization $\sigma_{\rm ion}$ to σ_+ change

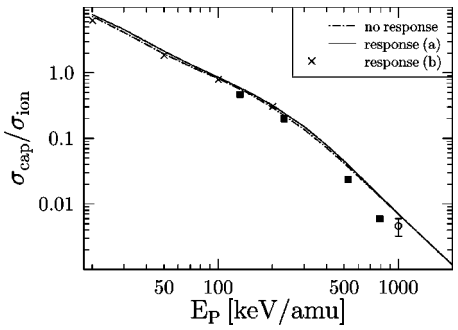

FIG. 4. Ratio of net electron capture σ_{cap} and net ionization σ_{ion} cross sections as a function of impact energy. Theory: present calculations for $C^{4+}+Ne$ collisions in the *no-response* approximation [Eq. (6)], with inclusion of the target-response potential (11) [response(a)] only, and with the additional projectile-response potential (17) [response(b)]. Experiment: F^{4+} projectiles; closed squares (error bars are within the size of the symbols) [21], (○) [22].

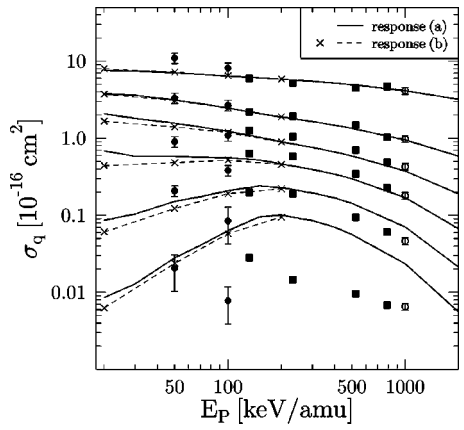

FIG. 5. Total cross section for q-fold electron loss σ_q ($q=1,\ldots,6$) as a function of impact energy. Theory: present calculations for $C^{4+}+Ne$ collisions with inclusion of the target-response potential (11) [response(a)] only, and with the additional projectile-response potential (17) [response(b)]. The theoretical data correspond to $q=1,\ldots,6$ from top to bottom. Experiment: C^{4+} projectiles; (●) [20], F^{4+} projectiles; closed squares (error bars are within the size of the symbols) [21], (○) [22].

significantly as a function of impact energy. In Fig. 4, we show the calculated ratio $\sigma_{cap}/\sigma_{ion}$ for $C^{4+}+Ne$ collisions in comparison with the experimental data for F^{4+} impact [21,22], for which this information could be extracted from the reported charge-state correlated cross sections. As mentioned in the discussion of Fig. 1, we have excluded the K shell of the projectile in the calculation of the capture, since we assume it to be occupied throughout the collision. Nevertheless, density may be transferred into this shell during the time propagation, as Pauli blocking due to the projectile electrons is not incorporated in the present calculations. We note, however, that this can be done on the level of the IPM by also propagating the projectile electrons and combining their transition amplitudes with the transition amplitudes of the target electrons on the basis of the *inclusive probabilities* formalism [26,31].

The agreement between the theoretical and experimental ratios $\sigma_{cap}/\sigma_{ion}$ displayed in Fig. 4 is very good. This confirms that it is reasonable to compare C^{4+}-impact data with F^{4+}-impact data for the global cross sections. It also indicates that the discrepancies observed for σ_+ (Fig. 2) are likely to be caused by the experimental problem to put the measurements on an absolute scale. We note that the *no-response* approximation and the two response models give very similar results for this ratio, which implies that overall, the response models reduce the total capture and ionization cross sections approximately by the same percentage.

We now turn to the more detailed cross sections for the production of recoil ions in specific charge states and for charge-state correlated events. In view of the apparent experimental uncertainties in the total net electron loss cross sections (Fig. 2), we have renormalized the experimental data shown in Figs. 5 to 7 to the theoretical net electron loss calculated in the *target-response* model.

In Fig. 5 we display the q-fold electron loss from the target, i.e., the cross sections for the production of recoil ions in the charge states q. The theoretical results are obtained by calculating cross sections for k-fold capture with simultaneous l-fold ionization σ_{kl} according to the analysis in terms of products of binomials [16] and adding them in the following way:

$$\sigma_q=\sum_{k+l=q}\sigma_{kl}\,. \tag{24}$$

We show only results obtained in the dynamical screening models in Fig. 5 for the sake of clarity, but note that similarly, as in our previous study of $He^{2+}+Ne$ collisions [18], the *no-response* cross sections are considerably larger than these data for the higher-recoil ion charge states q at low to intermediate impact energies. The displayed theoretical data are in very good agreement with the renormalized measurements of Refs. [21,22] for $q=1,\ldots,4$ and in acceptable agreement for $q=5$. Only for the highest charge state $q=6$, do they lie significantly above the experimental results. Whether this discrepancy would be reduced in a more refined dynamical screening model, or whether it cannot be resolved at all within an IPM, remains open at present.

At lower impact energies we observe discrepancies between our results and the measurements of Ref. [20]. The experimental relative contributions of the higher charge states ($q\geqslant 3$) are substantially smaller than the theoretical ones, in particular at 50 keV/amu. Inclusion of the projectile response potential reduces the cross sections for higher q only slightly and does not lead to an improved agreement. A closer inspection of our data for, e.g., $q=4$, shows that the dominant contribution is due to threefold capture with one-fold ionization σ_{31} followed by σ_{22} and σ_{40}. This is true for both dynamical screening models, although the projectile response reduces the threefold- and fourfold-capture processes substantially. By applying the formalism of *inclusive probabilities* [31], we have checked that the Pauli principle does not change these results significantly, since eight vacancies are available in the projectile L shell to which the target electrons are dominantly transferred. Unfortunately, the indi-

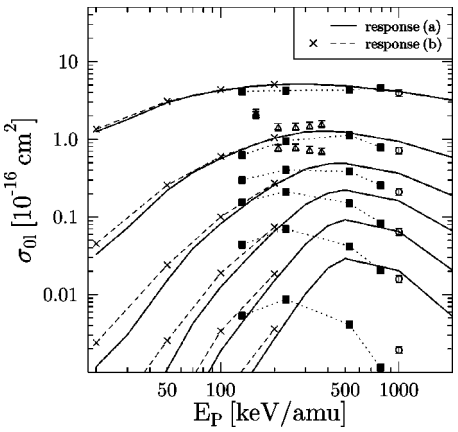

FIG. 6. Total cross section for pure l-fold ionization σ_{0l} ($l=1,\ldots,6$) as a function of impact energy. Theory: present calculations for $C^{4+}+Ne$ collisions with inclusion of the target-response potential (11) [response(a)] only, and with the additional projectile-response potential (17) [response(b)]. The theoretical data correspond to $l=1,\ldots,6$ from top to bottom. Experiment: F^{4+} projectiles; closed squares (error bars are within the size of the symbols) [21], (○) [22], (△) [32] for $l=2,3$ only. The data of Ref. [32] were normalized to the calculated single-ionization cross section σ_{01}, as only ratios of double to single and triple to single ionization are provided in Ref. [32].

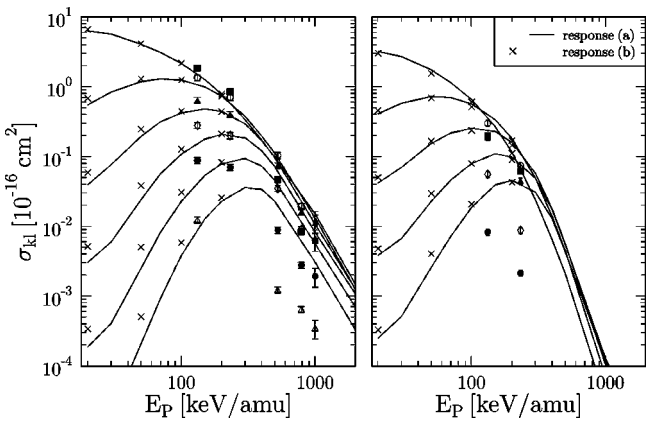

FIG. 7. Total cross section for single capture with simultaneous l-fold ionization σ_{1l} ($l=0,\ldots,5$) (left panel), and for double capture with simultaneous l-fold ionization σ_{2l} ($l=0,\ldots,4$) (right panel) as a function of impact energy. Theory: present calculations for $C^{4+}+Ne$ collisions with inclusion of the target-response potential (11) [response(a)] only, and with the additional projectile-response potential (17) [response(b)]. The theoretical data correspond to $l=0,\ldots,5$ from top to bottom at low energies. Experiment: F^{4+} projectiles; closed squares $l=0$, (○) $l=1$, closed triangles $l=2$, (◇) $l=3$, (●) $l=4$, (△) $l=5$; the data at 1 MeV/amu are from Ref. [22], and the data at lower impact energies are from Ref. [21].

vidual cross sections σ_{kl}, which would allow a more detailed analysis of the observed discrepancies, were not measured by the authors of Ref. [20].

In Fig. 6 we show cross sections for pure multiple ionization σ_{0l} for $l=1,\ldots,6$. Our results are in good agreement with the experimental data for F^{4+} impact for $l=1,2$, but behave differently as a function of the projectile energy for the higher degrees of ionization. In addition to the data of Refs. [21,22], we have included measurements for double and triple ionization reported in Ref. [32]. These results are generally larger than the cross sections of Ref. [21], in particular for $l=3$. At the lowest impact energy $E_P=160$ keV/amu, they appear to be much too high as the $l=2$ and $l=3$ data points almost merge.

At high energies $E_P \gtrsim 1000$ keV/amu, our results for pure multiple ionization are essentially identical to the cross sections for q-fold electron loss shown in Fig. 5 since capture is negligible in this region. By contrast, the experimental data for pure ionization are smaller than the q-fold loss cross sections for the higher charge states and, as a consequence, smaller than our results. This can be attributed to electron loss from the F^{4+} projectile, which is not included in the experimental data displayed in Fig. 6, but which does contribute to the total production of recoil ions (Fig. 5) when it is accompanied by target ionization. We have checked that the cross sections for the higher degrees of ionization l are substantially increased and in better agreement with our results when the contributions from these processes are added. At lower impact energies, the experimental data for pure ionization are larger than our results for $l \geqslant 3$. In this region capture processes gain importance. When they occur simultaneously with electron loss from the projectile, they may yield the same final charge states as pure ionization events. In our analysis of the scattering system $He^+ + Ne$, in which one electron at the projectile center is actively involved, we found that such processes significantly change the final charge-state correlated cross sections in the low to intermediate energy range [26]. Therefore, we conjecture that the discrepancies in the present case are mainly associated with the different projectiles employed in the experiments and the calculations.

The problem of the different projectile species becomes even more apparent in the case of single- and multiple-capture processes. In these cases, the electrons in the L-shell of the F^{4+} projectile affect the results by modifying the orbital energies of the vacant states compared to the C^{4+} ion, and by undergoing inelastic transitions that change the final charge state distributions. In Fig. 7, we show cross sections for single and double capture accompanied by l-fold ionization. We have included the experimental data of Refs. [21,22], although a direct comparison with our theoretical results seems inappropriate. Qualitatively, we observe a similar behavior as in the case of pure multiple ionization (Fig. 6): at lower energies, the measurements exceed the calculated cross sections, whereas they lie below our results at high impact energies. They show a more rapid decrease for the pure capture channels ($l=0$) than for the transfer-ionization channels ($l \geqslant 1$) toward high energies. Qualitatively, this feature is reproduced by our calculations for double capture, and also for triple and fourfold capture displayed in Fig. 8.

Finally, we briefly discuss the influence of the additional projectile-response potential $\delta v_{ee}^{P}(t)$ on the charge-state correlated cross sections σ_{kl}. Pure multiple ionization and single capture with ionization are enhanced at low to

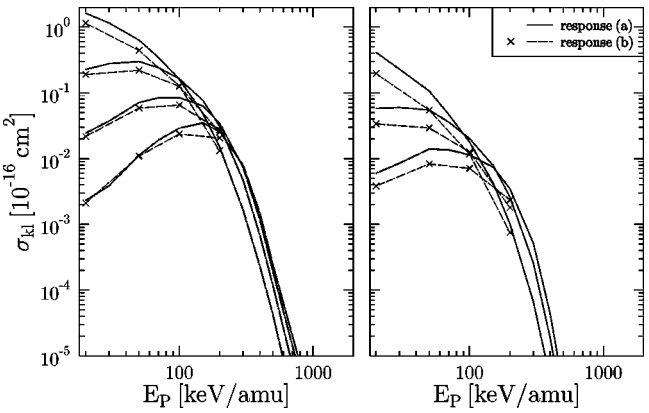

FIG. 8. Total cross section for threefold capture with simultaneous l-fold ionization σ_{3l} ($l=0,\ldots,3$) (left panel), and for fourfold capture with simultaneous l-fold ionization σ_{4l} ($l=0,\ldots,2$) (right panel) as a function of impact energy. Theory: present calculations for $C^{4+}+Ne$ collisions with inclusion of the target-response potential (11) [response(a)] only, and with the additional projectile-response potential (17) [response(b)]. The theoretical data correspond to $l=0,\ldots,3$ from top to bottom at low energies.

intermediate impact energies when $\delta v_{ee}^{P}(t)$ is included in the calculation, whereas multiple capture processes are reduced in this model. This reflects that the main effect of the dynamical screening of the projectile is a redistribution of the σ_{kl} from higher to lower k, while the global net cross sections (cf. Figs. 2 and 4) are only slightly modified. However, the effect is not very strong for the system considered here.

IV. CONCLUDING REMARKS

In this paper, we have presented theoretical results for charge-changing cross sections in $C^{4+}+Ne$ collisions at impact energies ranging from 20 to 2000 keV/amu. The calculations are based on the independent particle model (IPM). Time-dependent screening effects at the target and the projectile centers are included in terms of global response potentials $\delta v_{ee}^{T}(t)$ and $\delta v_{ee}^{P}(t)$, which are driven by the net electron loss and the net electron capture, respectively. The response potentials are designed to account for the increasing attraction of the target and the time-dependent screening of the projectile for *multiple*-electron ionization and capture, whereas their magnitudes are small in the kinematical range, in which *single*-electron processes dominate.

As in our previous study of $He^{2+}+Ne$ collisions [18], we have found that $\delta v_{ee}^{T}(t)$ significantly reduces the net electron loss at low to intermediate impact energies since multiple-electron processes are strongly suppressed. Inclusion of $\delta v_{ee}^{P}(t)$ modifies the global cross sections only slightly, but its influence on the results is noticeable on the level of the relative contributions of the single- and multiple-electron capture channels.

The comparison of our results with experimental data for C^{4+} and F^{4+} impact reveals some serious discrepancies, which are not likely to be explained by the limitations of our theoretical description. In particular, the experimental results for the net electron loss show structures in the energy dependence, which are beyond the quoted uncertainties, and which are not supported by measurements for collision systems with other projectile charges. This was concluded from plotting the net electron loss divided by the projectile charge as a function of the impact energy divided by the projectile charge. In such a plot, the results for collisions at the same reduced projectile energies should be comparable. Although systematic structures are not supported by the measurements available in the kinematical range of interest for the present paper, the data scatter considerably around our theoretical results, which, in contrast, are very similar for different projectiles. An important finding from the present calculations with target response is the fact that a universal effective scaling law is predicted for the net electron loss cross section at low to intermediate scaled energies over a substantial range of projectile charges. Experimental data with appropriate absolute normalization accuracy to verify this scaling are highly desirable.

For the q-fold electron loss, we found good agreement with the experimental data for F^{4+} impact, when the measurements were normalized to the calculated net electron loss. By contrast, discrepancies with measurements for C^{4+} collisions at lower projectile energies remain unexplained at present. Experimental charge-state correlated data were only reported for F^{4+} collisions, and were found to differ considerably from our calculations for C^{4+} impact. We believe that these discrepancies are mainly caused by the more active role of the projectile electrons in the case of F^{4+} projectiles.

In summary, we would like to point out that new accurate measurements of charge-state correlated and global cross sections are needed to clarifiy these issues and to assess the level of sophistication that is necessary for a quantitative description of many-electron scattering systems in terms of quantum-mechanical calculations. This information would also be helpful for an extension of the theoretical methods to the description of more differential observables, such as electron emission spectra in multiple-ionization processes. Our work demonstrates that detailed total cross section calculations in the nonperturbative realm have become possible in the framework of the IPM. In view of the limited reliable experimental information, we can only speculate at present about the overall quality of the response models used and the validity of the IPM to describe charge-state correlated cross sections in collisions of multiple charged ions with many-electron atoms.

ACKNOWLEDGMENTS

This work has been supported in part by the Natural Sciences and Engineering Research Council of Canada. T.K. gratefully acknowledges financial support of the DAAD.

[1] C.L. Cocke, Phys. Rev. A **20**, 749 (1979).
[2] C.L. Cocke and R.E. Olson, Phys. Rep. **205**, 153 (1991).
[3] J. Ullrich *et al.*, J. Phys. B **30**, 2917 (1997); R. Dörner *et al.*, Phys. Rep. **330**, 95 (2000).
[4] M.E. Rudd, Y.-K. Kim, D.H. Madison, and J.W. Gallagher, Rev. Mod. Phys. **57**, 965 (1985); R.D. DuBois and S.T. Manson, Phys. Rev. A **35**, 2007 (1987).
[5] R.D. DuBois, Phys. Rev. A **36**, 2585 (1987); **39**, 4440 (1989).
[6] R. K. Janev, L. P. Presnyakov, and V. P. Shevelko, *Physics of Highly Charged Ions*, Electrophysics Vol. 13 (Springer, Berlin, 1985); V. Shevelko and H. Tawara, *Atomic Multielectron Processes*, Atoms and Plasmas Vol. 23 (Springer, Berlin, 1998).
[7] R.E. Olson, J. Phys. B **12**, 1843 (1979).
[8] M. Horbatsch, J. Phys. B **25**, 3797 (1992).
[9] N.M. Kabachnik, V.N. Kondratyev, Z. Roller-Lutz, and H.O. Lutz, Phys. Rev. A **56**, 2848 (1997).
[10] B. H. Bransden and M. R. C. McDowell, *Charge Exchange and the Theory of Ion-Atom Collisions* (Claredon, Oxford, 1992), Chap. 8.4; S. Keller, H. Ast, and R.M. Dreizler, J. Phys. B **26**, 737 (1993); C.O. Reinhold and J. Burgdörfer, *ibid.* **26**, 3101 (1993).
[11] J. -P. Blaizot and G. Ripka, *Quantum Theory of finite Systems* (MIT Press, Cambridge, 1986), Chap. 9; P. Ring and P. Schuck, *The Nuclear Many-Body Problem* (Springer, New York, 1980), Chap. 12.
[12] E. K. U. Gross, J. F. Dobson, and M. Petersilka, in *Topics in Current Chemistry*, edited by R. F. Nalewajski (Springer, Heidelberg, 1996), Vol. 181, p. 81.
[13] K. Gramlich, N. Grün, and W. Scheid, J. Phys. B **19**, 1457 (1986); W. Stich, H.J. Lüdde, and R.M. Dreizler, Phys. Lett. **99A**, 41 (1983).
[14] C. Bottcher, Nucl. Instrum. Methods Phys. Res. B **10/11**, 7 (1985); R. Nagano, K. Yabana, T. Tazawa, and Y. Abe, Phys. Rev. A **62**, 062 721 (2000).
[15] T. Kirchner, L. Gulyás, H.J. Lüdde, A. Henne, E. Engel, and R.M. Dreizler, Phys. Rev. Lett. **79**, 1658 (1997); T. Kirchner, L. Gulyás, H.J. Lüdde, E. Engel, and R.M. Dreizler, Phys. Rev. A **58**, 2063 (1998).
[16] T. Kirchner, H.J. Lüdde, and R.M. Dreizler, Phys. Rev. A **61**, 012 705 (2000).
[17] T. Kirchner, H.J. Lüdde, M. Horbatsch, and R.M. Dreizler, Phys. Rev. A **61**, 052 710 (2000).
[18] T. Kirchner, M. Horbatsch, H.J. Lüdde, and R.M. Dreizler, Phys. Rev. A **62**, 042 704 (2000).
[19] H.J. Lüdde, A. Henne, T. Kirchner, and R.M. Dreizler, J. Phys. B **29**, 4423 (1996); O.J. Kroneisen, H.J. Lüdde, T. Kirchner, and R.M. Dreizler, J. Phys. A **32**, 2141 (1999).
[20] Y. Sugizaki, M. Sataka, K. Kawatsura, T. Shirai, and Y. Nakai, J. Phys. B **22**, 263 (1989).
[21] S. Kelbch *et al.*, J. Phys. B **23**, 1277 (1990).
[22] O. Heber *et al.*, Phys. Rev. A **52**, 4578 (1995).
[23] J.D. Talman and W.F. Shadwick, Phys. Rev. A **14**, 36 (1976); E. Engel and S.H. Vosko, *ibid.* **47**, 2800 (1993); E. Engel and R.M. Dreizler, J. Comput. Chem. **20**, 31 (1999).
[24] D. Elizaga *et al.*, J. Phys. B **32**, 857 (1999).
[25] A. A. Radzig and B. M. Smirnov, *Reference Data on Atoms, Molecules, and Ions*, Chemical Physics Vol. 31 (Springer, Berlin, 1985).
[26] T. Kirchner and M. Horbatsch, Phys. Rev. A (to be published).
[27] A.S. Schlachter *et al.*, Phys. Rev. A **23**, 2331 (1981).
[28] S.H. Be *et al.*, J. Phys. B **19**, 1771 (1986).
[29] J. Ullrich, K. Bethge, S. Kelbch, W. Schadt, H. Schmidt-Böcking, and K.E. Stiebing, J. Phys. B **19**, 437 (1986).
[30] T. Matsuo *et al.*, Phys. Rev. A **60**, 3000 (1999).
[31] H.J. Lüdde and R.M. Dreizler, J. Phys. B **18**, 107 (1985); P. Kürpick, H.J. Lüdde, W.D. Sepp, and B. Fricke, Z. Phys. D: At., Mol. Clusters **25**, 17 (1992).
[32] X. Cai *et al.*, Eur. Phys. J. D **6**, 23 (1999).
[33] H.M. Hellmann and E. Träbert, Phys. Rev. A **36**, 4085 (1987).
[34] J. Freyou, M. Breinig, C.C. Gaither III, and T.A. Underwood, Phys. Rev. A **41**, 1315 (1990).